OPEN

A glucose carbonate apatite complex exhibits *in vitro* and *in vivo* anti-tumour effects

Hirofumi Yamamoto[1], Xin Wu[1,2], Hiroyuki Nakanishi[3], Yuki Yamamoto[3], Mamoru Uemura[1], Taishi Hata[1], Junichi Nishimura[1], Ichiro Takemasa[1], Tsunekazu Mizushima[1], Jun-Ichi Sasaki[4], Satoshi Imazato[4], Nariaki Matsuura[5], Yuichiro Doki[1] & Masaki Mori[1]

[1]Department of Surgery, Gastroenterological Surgery, Graduate School of Medicine, Osaka University, Japan, [2]Research Fellow of Japan Society for the Promotion of Science, [3]Nakanishi Gastroenterological Research Institute, Japan, [4]Department of Biomaterials Science, Graduate School of Dentistry, Osaka University, Japan, [5]Osaka Medical Center for Cancer and Cardiovascular Diseases, Japan.

Tumour targeting nanotechnology has recently made therapeutic progress and several therapeutic nanoparticles have been approved for clinical application. However, an ideal nanotechnology based therapeutic for solid tumours, particularly for systemic administration, still remains a challenge in clinical cancer therapy. We previously reported a pH sensitive *in vivo* delivery system of doxorubicin, or microRNA, using carbonate apatite (CA) nanoparticles. To further explore utility of CA in cancer therapy, we attempted to transport excess glucose into tumour cells by conjugating glucose (Glc) to the nanoparticle. Despite the non-toxicity of CA and Glc, the complex (CA-[Glc]) exhibited an unexpected anti-cancer effect *in vitro* and *in vivo*. CA-[Glc] significantly reduced the growth of colon cancer cell lines. Intravenous injections successfully suppressed solid tumour growth. In mice and monkeys, intravenously injected CA-[Glc] complex resulted in no serious abnormalities in body weight or blood chemistry. Because cancer cells intensively metabolise glucose than normal cells, treatment of cancer using glucose seems paradoxical. However, with the aid of CA, this safe and 'sweet' complex may be a novel anti-cancer reagent.

N anotechnology has the potential to surmount the limitations of current cancer therapeutics[1]. Systemically administered engineered nanoparticles provide the opportunity to deliver reagents more precisely to tumour tissues, reducing toxicity to normal organs and enhancing anti-cancer effects compared with the incorporated reagents alone[2,3]. Nanoparticles of 100 nm are considered optimal for the passive targeting of tumours *in vivo*[4] due to the enhanced permeability and retention (EPR) effect, which is characterised by increased microvasculature leakage and impaired lymphatic function in tumours[5]. Despite decades of development, few therapeutic nanoparticles have been approved for clinical applications[6]. An ideal nanotechnology based therapeutic for solid tumours, particularly for systemic administration, still remains unrealised in clinical cancer therapy[7].

Previously, we introduced carbonate apatite (CA), which consisted of inorganic ions (CO_3^{2-}, Ca^{2+}, and PO_4^{3-}), as a pH sensitive delivery system for doxorubicin[8] or microRNA[9] that quickly accumulates in tumours after systemic administration. CA nanoparticles enter the cell via endocytosis within 1 h and are dissolved in the acidic pH of endosomes[8]. Intravenously administered CA-microRNA nanoparticles markedly accumulated in the tumour at 1 h and microRNA-340 delivered by CA significantly inhibited *in vivo* tumour growth[9]. It is well known that nanoparticles with incorporated reagents within cells must escape at the earliest opportunity from increasingly acidic endosomes; otherwise, the reagents will be further acidified and inactivated by lysosomes[10,11]. Therefore, the pH-sensitivity of CA is advantageous.

Cancer cells metabolise more glucose (Glc) than normal cells, known as the Warburg effect, and have upregulated glucose transporters, notably GLUT-1[12–14]. 18F-FDG, as a glucose analogue, is an agent that was designed based on this effect and has been used clinically to detect tumour tissue by PET-CT[15]. To achieve higher accumulation in tumour tissue, Tanaka *et al.* reported that a glucose-linked photosensitiser was a useful delivery system as a novel photodynamic therapy. These approaches are feasible due to glucose uptake via GLUT receptors[16,17].
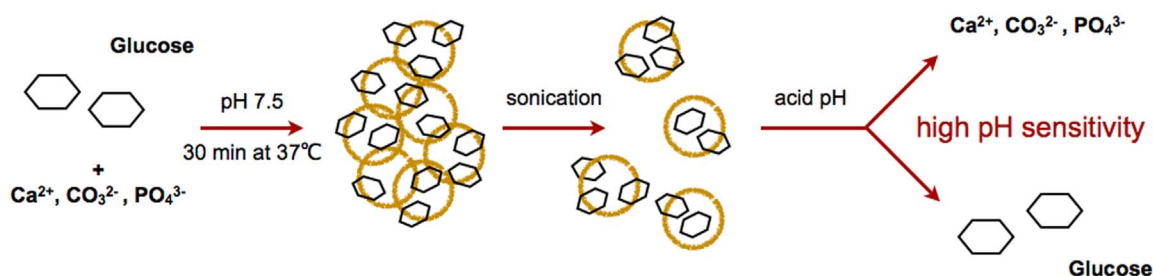
Figure 1 | Glucose carbonate apatite (CA-[Glc]) complex schematic. The generation process is simple, involving a mixture of the inorganic ions CO_3^{2-}, Ca^{2+}, PO_4^{3-} and glucose and incubation at 37°C for 30 min. After sonication, the complex forms at the nano-scale and is degradable at acidic pH to release the incorporated compounds.

Owing to the highly efficient intracellular delivery of CA, we attempted to transport excess Glc into tumour cells using CA nano-particles incorporating glucose (CA-[Glc]) in an effort to explore utility of CA in cancer therapy. As results, we observed a greater anti-tumour effect than we had expected. Although GLUT transporters influx glucose, the CA-[Glc] complex may allow greater amounts of glucose to be transferred into cells via clathrin-mediated endocytosis[18]. To explore the underlying mechanism, we measured the reactive oxygen species (ROS) activity because glucose-induced cytotoxicity is usually associated with the formation and regulation of ROS[19].

Results and Discussion

CA-[Glc] complex properties. The CA-[Glc] complex consists of inorganic ions (i.e., CO_3^{2-}, Ca^{2+}, and PO_4^{3-}) that are pH sensitive and degradable at an acidic pH, resulting in the release of incorporated compounds (Figure 1). The ^{13}C NMR spectra of CA, CA-[Glc] and Glc are shown in Figure 2a. A peak at 168 ppm was detected as the carbonate group in the CA sample and peaks at 60 ~ 100 ppm were detected as glucose in the Glc sample. These peaks were detected in the CA-[Glc] sample, suggesting the complex contains both CA and Glc. The complex size was 22.27 ± 5.10 nm (mean ± SD) and section images, measured by atomic force microscopy (AFM), are shown in Figure 2b. It has been demonstrated that intravenously administered nanoparticles larger than 100 nm are likely to be captured by the liver and spleen[20,21]. The small size of the CA-[Glc] nanoparticle is advantageous for avoiding reticuloendothelial system (RES) clearance. A diameter size larger than 5 nm was also necessary because it has been demonstrated that nanoparticles smaller than 5.5 nm are subject to capture in renal glomeruli[22]. Perrault reported that 100 nm PEGylated gold nanoparticles accumulated around the perivascular space, but 20 nm particles permeated tumours far from the vessel centers[23]. In a recent report detailing 30 nm micellar nanomedicines, Cabral stated that small sized nanoparticles were more advantageous than larger nanoparticles for penetrating poorly permeable hypovascular tumours[24]. The CA-[Glc] complexes have a similar size, 10–30 nm, as the RNA packaging nanoparticles developed by Guo et al. that have demonstrated efficient siRNA delivery to solid tumours[25–28].

The zeta potential of CA-[Glc], when incubated in 4 mM Ca^{2+}-supplemented bicarbonate buffer, was observed to be −9.06 ± 1.07 mV (mean ± SD; n = 5) (Figure 2c). Complexes with a positive surface charge, such as liposomes or micelles, aggregate with anionic serum proteins. This results in accumulation in the lung and causes nonspecific uptake by the RES[29]. The negative zeta potential of CA-[Glc] would not assemble anionic serum proteins and would avoid accumulation in the glomerular basement membrane due to charge repulsion[30].

Moreover, the CA-[Glc] complex was pH sensitive (Figure 2d). The complex was gradually degraded as pH decreased from 8.0. Below pH 7.0, the complex was completely degraded. Many nanoparticles enter cells through endocytosis and the delivered compounds must escape at the earliest opportunity from increasingly

acidic endosomes; otherwise, the compounds are further acidified and inactivated by their relocation to lysosomes[10,11,31]. An effective mechanism to facilitate endosomal escape is pH sensitivity.

The conjugated amount of Glc in CA was 25.0 mg, 12.0 mg, or 3.4 mg when 12.5 g, 6.25 g, or 2.5 g Glc was added during complex formation, respectively (Figure 2e). Thus the binding affinity of Glc to CA was 0.20% when 12.5 g of Glc was added during complex formation.

CA-[Glc] complex mediated cytotoxicity in colon cancer cells. We examined *in vitro* growth inhibition with treatment of CA and glucose (CA + Glc) or CA-[Glc]. Although CA + Glc did not inhibit cell growth compared to CA alone, CA-[Glc] containing the same concentration of Glc significantly largely inhibited the growth of HCT116 and HT29 cells at 48 h (Figure 3a, b).

Glucose-induced cytotoxicity is usually associated with the formation and regulation of reactive oxygen species (ROS)[19]. In order to get a better understanding of the underlying mechanism, we measured ROS activity. The relative ROS intensity in the HCT116 cells treated with CA-[Glc] was significantly higher than those treated with CA + Glc, at both 24 and 48 h (Figure 3c). However, the ROS activity of CA + Glc was not enhanced as compared to CA alone. Similar results were noted in HT29 cells. The significantly higher ROS in the cells treated with CA-[Glc] may partially support the CA-[Glc] complex mediated cytotoxicity in colon cancer cells. This unexpected cytotoxic effect may be explained by the small size and pH-sensitivity of CA-[Glc]. Smaller complexes are generally more efficiently taken up by endocytosis[32]. As shown in Figure 2b, the CA-[Glc] complex was 20 nm in size, which may enhance cellular uptake. After endocytosis, CA-[Glc] rapidly releases Glc due to the low endosomal pH, as demonstrated by the pH-sensitivity assay where we observed complete degradation of the complex below pH 7.2.

CA-[Glc] *in vivo* anti-tumour effect. In the mouse therapeutic model of pre-established HCT116 tumours, CA-[Glc] complex containing 50 mg glucose, CA, Glc (50 mg glucose), or saline was intravenously injected through the tail vein, when the tumour volume reached approximately 80 mm[3], three times per week for 2 weeks. As shown in Figure 4, significantly stronger growth inhibition was noted in CA-[Glc] treated mice compared with others. On day 16, the tumour volume of mice treated with CA-[Glc] was significantly smaller than in mice treated with CA (P = 0.0282), Glc (P = 0.0282), or saline (P = 0.0072).

In order to evidence the tumour uptake of glucose facilitated by CA-[Glc], we intravenously injected CA-[Glc] complex containing 100 mg glucose and Glc (100 mg) in the mouse therapeutic model of pre-established head and neck FaDu tumours. The glucose in tumour treated with CA-[Glc] was significantly higher at 3 and 24 h than that treated with Glc (n = 4, P = 0.0265 for both, Supplementary Figure S1).

CA-[Glc] *in vivo* toxicity. To examine *in vivo* safety, we investigated the toxicity of CA-[Glc] at day 12 after a 7 day consecutive injections

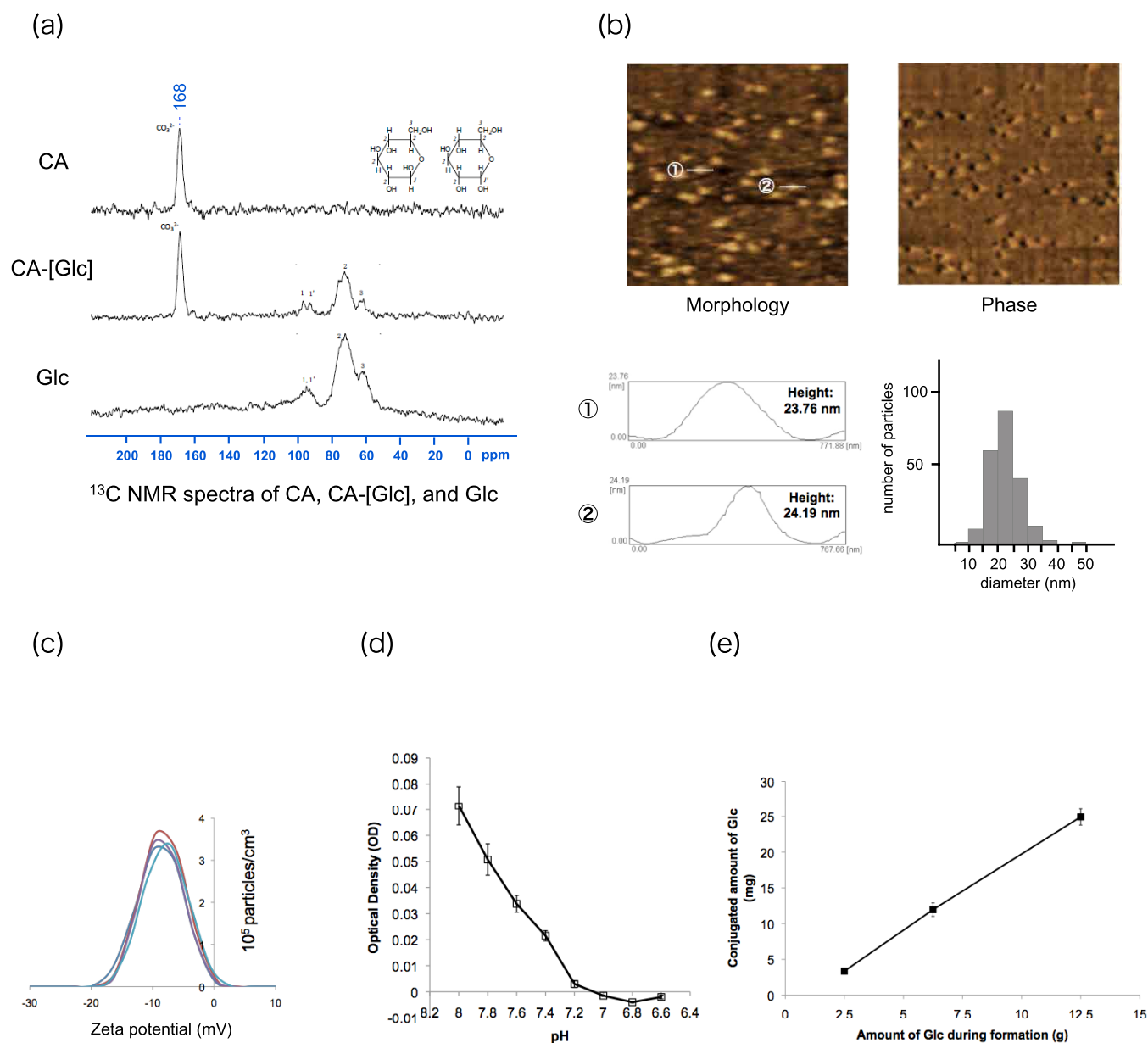**Figure 2 | Characterisation of glucose carbonate apatite (CA-[Glc]).** (a) The ^{13}C NMR spectrum of CA, CA-[Glc] and Glc. (b) Atomic force microscopy image of CA-[Glc] complex with cross-section profile and size distribution measured by atomic force microscopy. The complex size ranged from 10 to 40 nm (mean ± SD: 22.27 ± 5.10 nm). (c) Zeta potential (mV) of CA-[Glc] was observed to be −9.06 ± 1.07 mV (mean ± SD; n = 5). (d) pH sensitivity of CA-[Glc]. Below pH 7.0 the complex was completely degraded. (e) The conjugated amount of Glc in CA was 25.0 mg, 12.0 mg, or 3.4 mg when 12.5 g, 6.25 g, or 2.5 g Glc was added during complex formation, respectively.

of CA-[Glc] containing 100 mg of glucose. We observed no mortalities or body weight loss (Figure 5a). Blood chemistry tests revealed no physiologically significant differences between controls and CA-[Glc] treated groups (Figure 5b), except for the slight increase in BUN ($P = 0.0477$).

To demonstrate the potential utility of CA-[Glc] against human tumours, we should perform repeat injections to monkeys with appropriate controls for a long period. Prior to this stage, we preliminarily prepared an approximately 60-fold CA-[Glc] (for per injection corresponds to carry 2.5 g/kg glucose) of the mouse dose per injection for administration to monkeys for 4 consecutive days (n = 3) (Figure 5c). Monitored variables are listed in Supplementary Table 1–3. The monkeys' bodies were restricted for 30 min during CA-[Glc] i.v. injection. During and after injection, the general condition of monkeys was unremarkable and urine tests were normal. Blood tests were normal except for the following 3 items; two monkeys

(No.1 and No. 2) had increased serum AST with a peak on day 1. All monkeys had increased CPK levels, and isozyme analysis indicated that the majority was CPK-MM derived from skeletal muscle. All monkeys also had increased LDH levels with a distinct isozyme distribution. Although these enzymes were increased in monkeys, isoenzyme analysis suggested that they were unlikely derived from the heart or liver because cardiac muscle derived CPK-MB or liver associated LDH5 were not increased. Instead, skeletal muscle related CPK-MM and LDH1-2 were elevated. These abnormal values recovered to the normal range on day 10 (Figure 5c). The level of BUN was within normal range in monkeys.

Conclusion

It is suggested that CA-[Glc] may be a novel anti-cancer drug with no serious adverse events, and this effect could be at least in part due to upregulation of ROS activity.
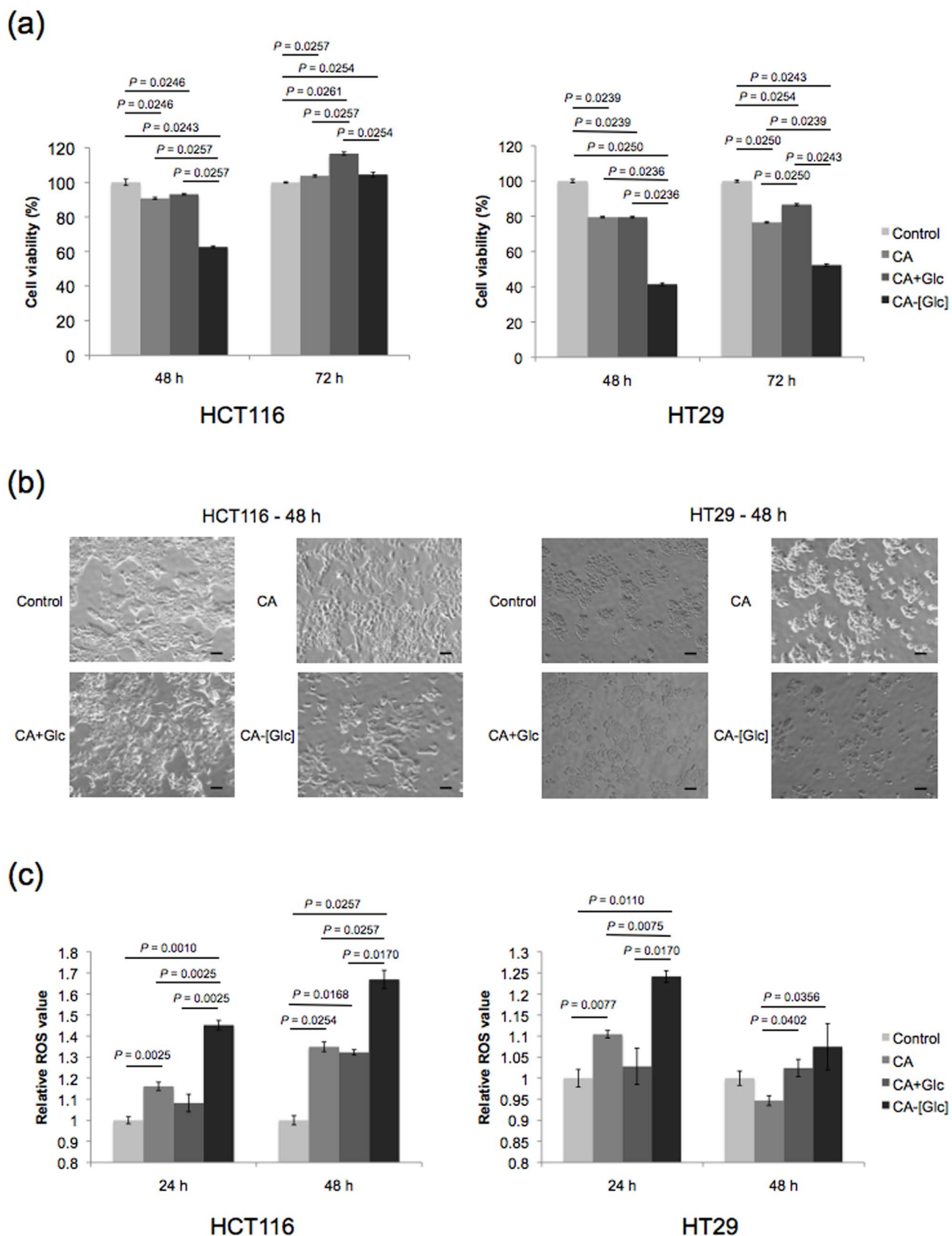
Figure 3 | *In vitro* cytotoxicity and ROS assay. (a) CA or CA + Glc treatment resulted in approximately 90% cell viability in HCT116 or HT29 cells at the indicated times. CA-[Glc] containing the same concentration of Glc or CA significantly reduced the growth of HCT116 cells to 60% viability at 48 h, or HT29 cells to 40 ~ 50%, at 48 and 72 h post-treatment (n = 6, Steel-Dwass All Pairs Test). (b) The cell morphology of CA, CA + Glc, or CA-[Glc] treated HCT116 and HT29 cells at 48 h. (c) The relative ROS intensity in the HCT116 or HT29 cells treated with CA-[Glc] showed significantly higher than those with CA or CA + Glc (n = 5 ~ 10, Steel-Dwass All Pairs Test).
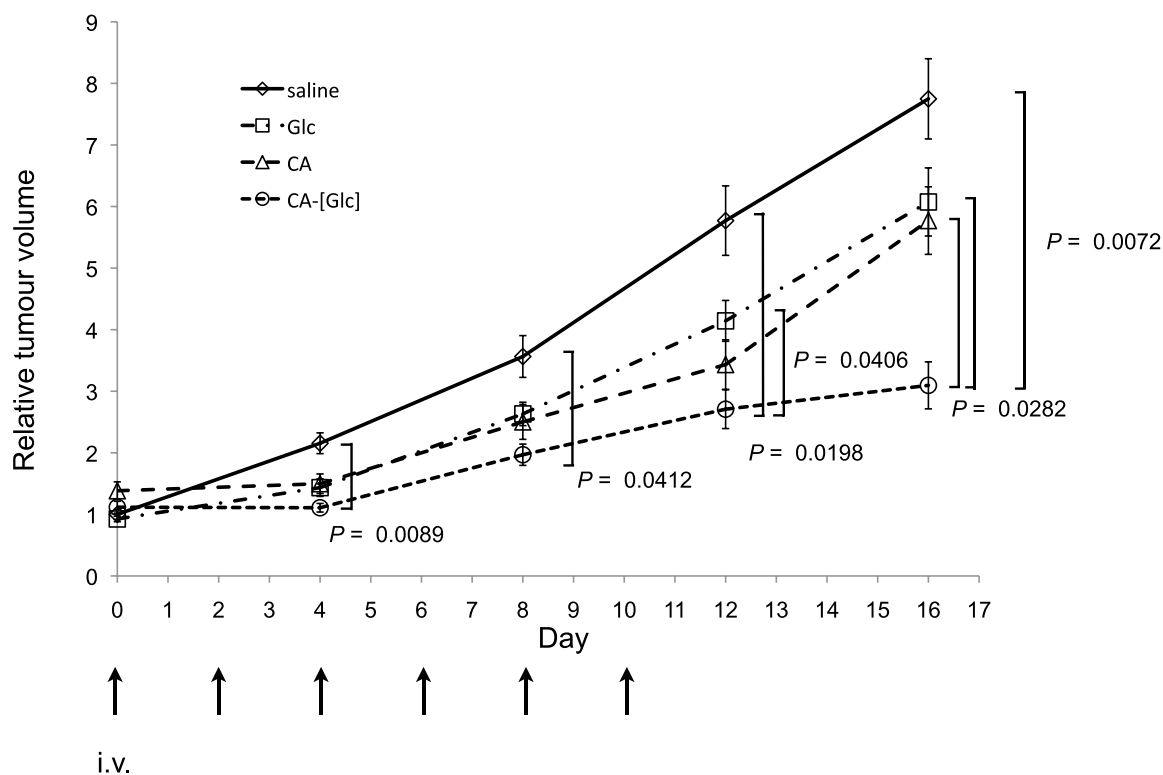
Figure 4 | *In vivo* anti-tumour effects of CA-[Glc]. In the mouse therapeutic model of pre-established HCT116 tumours, CA-[Glc] complex containing 50 mg glucose, CA, Glc (50 mg glucose), or saline was intravenously injected through the tail vein, when the tumour volume reached approximately 80 mm³, three times per week for 2 weeks. On day 16, the tumour volume of mice treated with CA-[Glc] was significantly smaller than in mice treated with CA ($P = 0.0282$), Glc ($P = 0.0282$), or saline ($P = 0.0072$). (n = 19 for saline, n = 8 for CA or Glc, n = 6 tumours for CA-[Glc], Steel-Dwass All Pairs Test).

Methods

Animals. Three- to 5-year-old female (2.51 to 2.60 kg, n = 3) *cynomolgus* monkeys (NAFOVANNY, Vietnam) were used at the animal testing facility of the Kannami Laboratory, Bozo Research Center Inc. This study was approved by the Animal Experiment Committee of the test facility.

Seven-week-old BALB/cAJcl-nu/nu nude mice were purchased from CLEA, Japan. The mice model study was performed in strict accordance with the recommendations in the Guide for the Care and Use of Laboratory Animals of Graduate School of Medicine, Osaka University. The protocol was approved by the Committee on the Ethics of Animal Experiments of Osaka University (Permit Number: 24-122-001, 23-023-001). All surgeries were performed under sodium pentobarbital anaesthesia and all efforts were made to minimise suffering.

Cell lines and reagents. Human colon cancer cell lines HCT116, HT29, and the FaDu human head and neck cancer cell line were purchased from the American Type Culture Collection. HCT116 and FaDu were grown in DMEM; HT29 was grown in RPMI supplemented with 10% foetal bovine serum (FBS), in 5% CO_2 at 37°C. $NaHCO_3$, $NaH_2PO_4 \cdot 2H_2O$ and $CaCl_2$ were purchased from Wako Pure Chemical Industries. DMEM powder was purchased from GIBCO.

Production of CA-[Glc]. $CaCl_2$ (4 μL, 1 M) was mixed in 1 mL of inorganic solution ($NaHCO_3$; 44 mM, NaH_2PO_4; 0.9 mM, $CaCl_2$; 1.8 mM, pH 7.5) with 50% glucose, followed by incubation at 37°C for 30 min. The solution was centrifuged at 12,000 rpm for 3 min and the pellet was dissolved with medium for *in vitro* transfection or saline containing 0.5% albumin for *in vivo* injection.

NMR measurements. NMR data were acquired at room temperature on a Bruker CXP 200 spectrometer operating at 50.3 MHz. Samples were spun at 3.0–3.5 kHz. The chemical shifts were referenced to the external chemical shift of the crystalline and amorphous POM resonances (both at 88.8 ppm). Typical cross polarisation parameters were: 4is, 1 ms contact time and a 4 s recycle time, collecting 2048 points in the time domain for a 20 kHz spectral width. Depending on the sample, 1000–15000 free induction decays were collected for the dipolar decoupling/cross polarisation/magic angle spinning experiments.

Morphology and size distribution analysis by atomic force microscopy. The morphology and size distribution of the CA-[Glc] complex was analysed using a scanning probe microscope (SPM-9500, Shimadzu) in dynamic mode, equipped with a microcantilever (OMCL-AC240TS-R3, Olympus). All samples were air dried for 5 min and analysed on freshly cleaved mica substrate.

Zeta potential measurement. The zeta potential of CA was measured by Laser Doppler Micro-electrophoresis (Zetasizer Nano Z, Malvern) at 25°C for 30 sec.

Estimation of the dissolution of CA-[Glc] complex at different pH values. Optical density (OD) at 655 nm of the samples was measured at different pH spectrophotometrically using a microplate reader (680 XR, Bio-Rad).

Cell proliferation assay. HCT116 cells were uniformly seeded into 96-well plates (1 × 10⁴ cells/well). Cell counting was performed using OneCell Counter (BioMedicalScience).

ROS assay and flow cytometric analysis. To measure reactive oxygen species (ROS), we used a cell-permeant dye CellROX™ Deep Red reagent (Invitrogen). Cells were treated without or with CA, CA + Glc, or CA-[Glc] for 24 and 48 h. Five μM CellROX™ Deep Red reagent was added to the cultures for 30 min. After washing with PBS, the fluorescence with absorption/emission maxima at ~644/665 nm were measured by flow cytometric analysis using a BD FACS Aria II instrument (BD Biosciences). The data were analyzed using BD FACS Diva software (BD Biosciences).

Anti-tumour activity assay. Human colon cancer HCT116 cells (5.0 × 10⁶ cells) were inoculated subcutaneously in the left and right flanks of mice to establish the solid tumour model. Systemic injections began when HCT116 tumour volumes reached approximately 80 mm³ with administration of saline, CA, Glc (50 mg) or CA-[Glc] complex containing 50 mg glucose. Mice were treated three times per week for 2 weeks. Anti-tumour activity was evaluated by tumour size, which was estimated using the following equation: V = a × b²/2, where a and b represent the major and minor axes of the tumour, respectively.

In vivo toxicity study on CA in mice. Mice were treated for a 7 day consecutive injections of CA-[Glc]. On day 12, mice were sacrificed and blood was collected for serum chemistry analysis.

Non-human primate study. *Cynomolgus* monkeys received a 30 min CA-[Glc] i.v. infusion on day 1, 2, 3, and 4. The amount of CA-[Glc] for per injection corresponds to a dose of 2.5 g/kg glucose. The general condition, urinalysis, and blood chemistry examinations listed in Supplementary Table 1 were obtained at the indicated time points. The detailed contents of urine and blood examinations are shown in Supplementary Table 2 and 3.
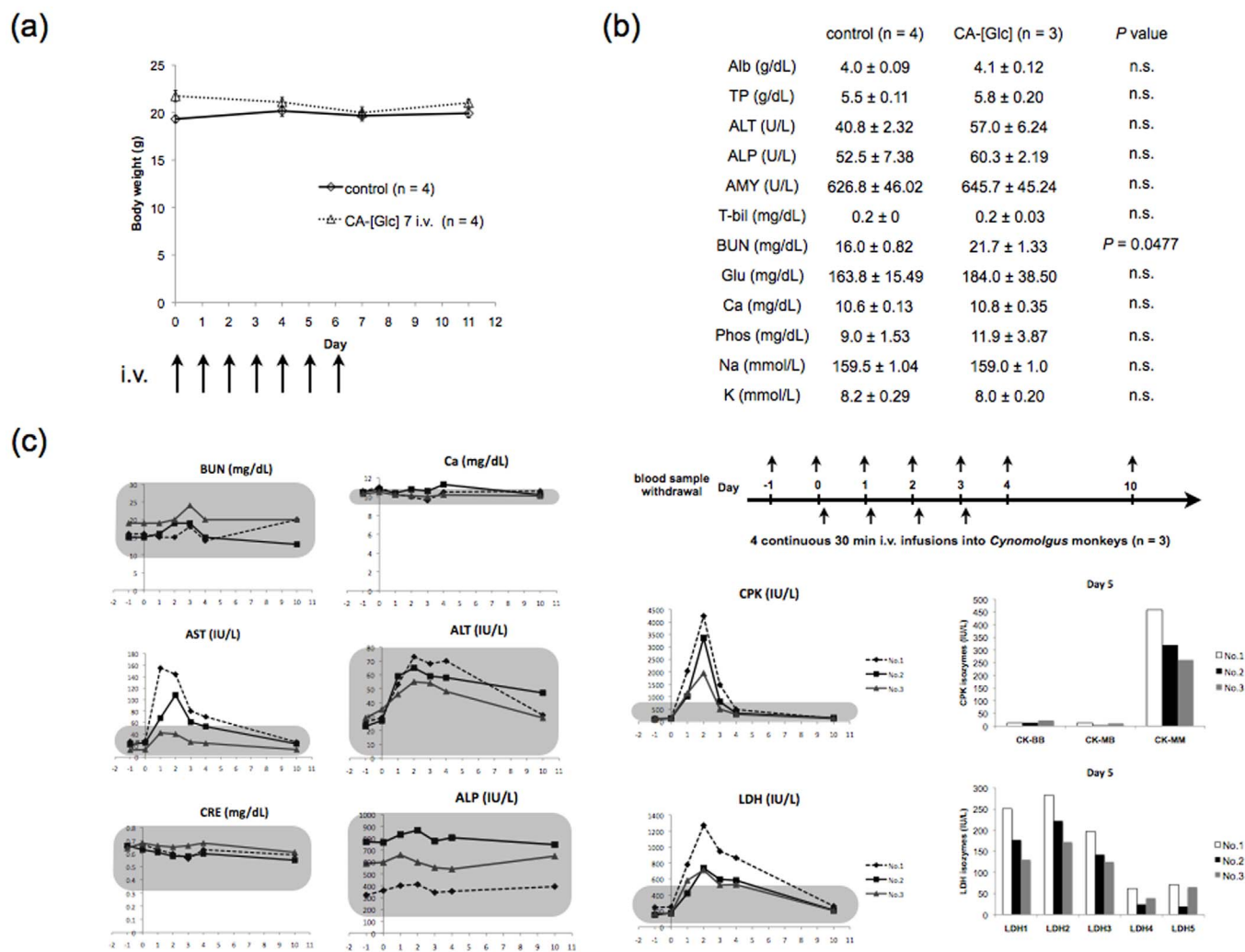
Figure 5 | CA-[Glc] toxicity. Mice were treated with intravenous injections of a CA-[Glc] complex containing 100 mg glucose for 7 consecutive injections. (a) Body weight curves of mice and (b) blood chemistry data for no treatment and CA-[Glc] treated mice (n = 3 ~ 4, Wilcoxon rank test). (c) Blood chemistry data (days −1 ~ 4 and day 10) of *Cynomolgus* monkeys (n = 3). Monkeys received a 30 min CA-[Glc] i.v. infusion on days 0, 1, 2, and 3. The amount of CA for per injection corresponds to a dose of 2.5 g/kg glucose. The grey rectangle area indicates normal ranges (mean ± 2 SD). Isoenzyme analysis of CPK and LDH from blood samples on day 5 are presented together. Each isoenzyme is derived from specific organs as follows: CPK-BB, brain; CPK-MB, cardiac muscle; CPK-MM, skeletal muscle; LDH1-2, cardiac muscle, skeletal muscle, red blood cell, and kidney; LDH5, liver, skin and muscle.

Statistical analysis. Statistical analyses were performed using the JMP10 program (SAS Institute). Data were expressed as the mean ± SD and analysed using the nonparametric Wilcoxon rank test in two groups comparison, and the nonparametric Steel-Dwass All Pairs Test dealing with multi comparisons. The results were considered statistically significant if two-tailed P-values were less than 0.05.

1. Petros, R. A. & DeSimone, J. M. Strategies in the design of nanoparticles for therapeutic applications. *Nat Rev Drug Discov* **9**, 615–627, doi:10.1038/nrd2591 (2010).
2. Davis, M. E., Chen, Z. G. & Shin, D. M. Nanoparticle therapeutics: an emerging treatment modality for cancer. *Nat Rev Drug Discov* **7**, 771–782, doi:10.1038/nrd2614 (2008).
3. Mao, C. Q. *et al.* A biodegradable amphiphilic and cationic triblock copolymer for the delivery of siRNA targeting the acid ceramidase gene for cancer therapy. *Biomaterials* **32**, 3124–3133, doi:10.1016/j.biomaterials.2011.01.006 (2011).
4. Perrault, S. D., Walkey, C., Jennings, T., Fischer, H. C. & Chan, W. C. Mediating tumor targeting efficiency of nanoparticles through design. *Nano Lett* **9**, 1909–1915, doi:10.1021/nl900031y (2009).
5. Matsumura, Y. & Maeda, H. A new concept for macromolecular therapeutics in cancer chemotherapy: mechanism of tumoritropic accumulation of proteins and the antitumor agent smancs. *Cancer Res* **46**, 6387–6392 (1986).
6. Peer, D. *et al.* Nanocarriers as an emerging platform for cancer therapy. *Nat Nanotechnol* **2**, 751–760, doi:10.1038/nnano.2007.387 (2007).
7. Pecot, C. V., Calin, G. A., Coleman, R. L., Lopez-Berestein, G. & Sood, A. K. RNA interference in the clinic: challenges and future directions. *Nat Rev Cancer* **11**, 59–67, doi:10.1038/nrc2966 (2011).
8. Hossain, S. *et al.* Fabrication and intracellular delivery of doxorubicin/carbonate apatite nanocomposites: effect on growth retardation of established colon tumor. *PLoS One* **8**, e60428, doi:10.1371/journal.pone.0060428 (2013).
9. Takeyama, H. *et al.* Decreased miR-340 expression in bone marrow is associated with liver metastasis of colorectal cancer. *Mol Cancer Ther* **13**, 976–985, doi:10.1158/1535-7163.MCT-13-0571 (2014).
10. Varkouhi, A. K., Scholte, M., Storm, G. & Haisma, H. J. Endosomal escape pathways for delivery of biologicals. *J Control Release* **151**, 220–228, doi:10.1016/j.jconrel.2010.11.004 (2011).
11. Dominska, M. & Dykxhoorn, D. M. Breaking down the barriers: siRNA delivery and endosome escape. *J Cell Sci* **123**, 1183–1189, doi:123/8/1183 (2010).
12. Warburg, O. On the origin of Cancer Cells. *Science* **123**, 309–314 (1956).
13. Koppenol, W. H., Bounds, P. L. & Dang, C. V. Otto Warburg's contributions to current concepts of cancer metabolism. *Nat Rev Cancer* **11**, 325–337, doi:10.1038/nrc3038 (2011).
14. Gatenby, R. A. & Gillies, R. J. Why do cancers have high aerobic glycolysis? *Nat Rev Cancer* **4**, 891–899 doi:10.1038/nrc1478 (2004).
15. Gambhir, S. S. Molecular imaging of cancer with positron emission tomography. *Nat Rev Cancer* **2**, 683–693, doi:10.1038/nrc882 (2002).
16. Tanaka, M. *et al.* Anticancer effects of novel photodynamic therapy with glycoconjugated chlorin for gastric and colon cancer. *Anticancer Res* **31**, 763–769 (2011).

17. Hirohara, S. *et al.* Sugar-dependent aggregation of glycoconjugated chlorins and its effect on photocytotoxicity in HeLa cells. *J Photochem Photobiol B* **84**, 56–63, doi:10.1016/j.jphotobiol.2006.01.011 (2006).

18. Nag, K., Hossain, S., Naznin, S. & Chowdhury, E. H. PKC activation promotes internalization of DNA-immobilized inorganic nano-crystals by clathrin-dependent endocytosis for efficient transgene expression in human lymphocytes. *Journal of Nanomedicine and Nanotechnology* **4**, 174, doi:10.4172/2157-7439.1000174 (2013).

19. Bonnefont-Rousselot, D. Glucose and reactive oxygen species. *Curr Opin Clin Nutr Metab Care* **5**, 561–568 (2002).

20. Pecot, C. V., Calin, G. A., Coleman, R. L., Lopez-Berestein, G. & Sood, A. K. RNA interference in the clinic: challenges and future directions. *Nat Rev Cancer* **11**, 59–67, doi:10.1038/nrc2966 (2011).

21. Miele, E. *et al.* Nanoparticle-based delivery of small interfering RNA: challenges for cancer therapy. *Int J Nanomedicine* **7**, 3637–3657, doi:10.2147/IJN.S23696 (2012).

22. Choi, H. S. *et al.* Renal clearance of quantum dots. *Nat Biotechnol* **25**, 1165–1170, doi: 10.1038/nbt1340 (2007).

23. Perrault, S. D., Walkey, C., Jennings, T., Fischer, H. C. & Chan, W. C. Mediating tumor targeting efficiency of nanoparticles through design. *Nano Lett* **9**, 1909–1915, doi:10.1021/nl900031y (2009).

24. Cabral, H. *et al.* Accumulation of sub-100 nm polymeric micelles in poorly permeable tumours depends on size. *Nat Nanotechnol* **6**, 815–823, doi:10.1038/nnano.2011.166 (2011).

25. Guo, P. The emerging field of RNA nanotechnology. *Nat Nanotechnol* **5**, 833–842, doi:10.1038/nnano.2010.231 (2010).

26. Haque, F. *et al.* Ultrastable synergistic tetravalent RNA nanoparticles for targeting to cancers. *Nano Today* **7**, 245–257, doi:10.1016/j.nantod.2012.06.010 (2012).

27. Shu, D., Shu, Y., Haque, F., Abdelmawla, S. & Guo, P. Thermodynamically stable RNA three-way junction for constructing multifunctional nanoparticles for delivery of therapeutics. *Nat Nanotechnol* **6**, 658–667, doi:10.1038/nnano.2011.105 (2011).

28. Shu, Y., Shu, D., Haque, F. & Guo, P. Fabrication of pRNA nanoparticles to deliver therapeutic RNAs and bioactive compounds into tumor cells. *Nat Protoc* **8**, 1635–1659, doi:10.1038/nprot.2013.097 (2013).

29. Tamura, A. & Nagasaki, Y. Smart siRNA delivery systems based on polymeric nanoassemblies and nanoparticles. *Nanomedicine (Lond)* **5**, 1089–1102, doi:10.2217/nnm.10.76 (2010).

30. Zuckerman, J. E., Choi, C. H., Han, H. & Davis, M. E. Polycation-siRNA nanoparticles can disassemble at the kidney glomerular basement membrane. *Proc Natl Acad Sci U S A* **109**, 3137–3142, doi:10.1073/pnas.1200718109 (2012).

31. Friend, D. S., Papahadjopoulos, D. & Debs, R. J. Endocytosis and intracellular processing accompanying transfection mediated by cationic liposomes. *Biochim Biophys Acta* **1278**, 41–50 (1996).

32. Jordan, M., Schallhorn, A. & Wurm, F. M. Transfecting mammalian cells: optimization of critical parameters affecting calcium-phosphate precipitate formation. *Nucleic Acids Res* **24**, 596–601 (1996).

Author contributions

H.Y. and X.W. developed the concept, designed the experiments, performed the animal experiments, analyzed the results and wrote the manuscript. H.N., Y.Y., J.S. and S.I. provided the NMR and AFM measurement. M.U., T.H., J.N., I.T. and T.M. performed *in vitro* proliferation assays. N.M., Y.D. and M.M. interpreted the results and edited the manuscript. All authors reviewed the manuscript.

Additional information

Supplementary information accompanies this paper at http://www.nature.com/scientificreports

Competing financial interests: The authors declare no competing financial interests.

How to cite this article: Yamamoto, H. *et al.* A glucose carbonate apatite complex exhibits *in vitro* and *in vivo* anti-tumour effects. *Sci. Rep.* **5**, 7742; DOI:10.1038/srep07742 (2015).